Vibrational Spectroscopy 103 (2019) 102935

Contents lists available at ScienceDirect

Vibrational Spectroscopy

journal homepage: www.elsevier.com/locate/vibspec

Temperature-induced phase transition of $Ca_2AlSiO_{5.5}$: Raman spectroscopic study

Shuangmeng Zhai[a,*], Kuan Zhai[a,b], Hu Wang[c], Xiang Wu[c], Weihong Xue[a]

[a] Key Laboratory of High-temperature and High-pressure Study of the Earth's Interior, Institute of Geochemistry, Chinese Academy of Sciences, Guiyang 550081, Guizhou, China

[b] University of Chinese Academy of Sciences, Beijing 100049, China

[c] State Key Laboratory of Geological Processes and Mineral Resources, China University of Geosciences, Wuhan 430074, China

ARTICLE INFO

Keywords:
$Ca_2AlSiO_{5.5}$
Phase transition
Raman spectra
High
Temperature

ABSTRACT

The Raman spectra of low-pressure and high-pressure $Ca_2AlSiO_{5.5}$ oxygen-deficient perovskites have been investigated in the temperature range of 153–1273 K at ambient pressure. No phase transition was observed for low-pressure $Ca_2AlSiO_{5.5}$ in this study, but an irreversible phase transition was observed for high-pressure $Ca_2AlSiO_{5.5}$ at 1223 K. The recovered sample of high-pressure $Ca_2AlSiO_{5.5}$ from 1273 K was confirmed as a single homogeneous phase (high-temperature $Ca_2AlSiO_{5.5}$). The Raman spectra of high-temperature $Ca_2AlSiO_{5.5}$ phase have also been studied in the temperature range of 153–1273 K at ambient pressure. All the observed Raman active bands of the three samples showed linear temperature dependence with different slopes. The quantitative temperature dependences of Raman bands are -2.90×10^{-2} ~ -0.31×10^{-2}, -3.56×10^{-2} ~ -0.50×10^{-2}, and -3.20×10^{-2} ~ 0.28×10^{-2} $cm^{-1} K^{-1}$ for low-pressure, high-pressure and high-temperature $Ca_2AlSiO_{5.5}$, respectively. The isobaric mode Grüneisen parameters of low-pressure $Ca_2AlSiO_{5.5}$ were calculated by using present high-temperature Raman spectra combined with a previous result of the thermal expansion coefficient, varying from 0.08 to 1.10 with an average of 0.35.

1. Introduction

Perovskite is one of the most important materials due to many interesting properties including ferroelectricity [1], piezoelectricity [2], charge ordering [3], superconductivity [4], colossal magnetoresistance [5], spin dependent transport [6], chemical catalysis [7], and high thermo power [8]. Numerous kinds of perovskite were synthesized with different applications. In earth science, pervoskite was widely investigated because it is the most abundant mineral [9].

The ideal stoichiometric perovskites ABX_3 consist of a three-dimensional framework of corner-sharing BX_6 octahedra, and the A-site fills the 12-fold cavities formed by the BX_3 network and is surrounded by 12 equidistant anions [10,11]. On the other hand, non-stoichiometric perovskites including hydroxide- and arsenide-based minerals are known as defect perovskites, characterized by A- and/or B-site vacancies together with the anion-deficient [11]. For example, the Si^{4+} cation in $CaSiO_3$ perovskite can be replaced by trivalent cations, such as Al^{3+} [12]. The mechanism can be expressed as $2Si^{4+} = 2Al^{3+} + Vö$, where Vö represents oxygen vacancy for balancing the charge [13]. Indeed, a high-pressure $Ca_2AlSiO_{5.5}$ oxygen-deficient perovskite (HP-$Ca_2AlSiO_{5.5}$) was synthesized at 1973 K and 16 GPa, in which 50% Si was replaced by Al [14]. The crystal structure of HP-$Ca_2AlSiO_{5.5}$ was determined as a rhombohedral defect perovskite with a five-fold superstructure developed along the pseudo-cubic {111} direction, and the Si and Al distributed randomly in octahedral sites [14]. Later a low-pressure $Ca_2AlSiO_{5.5}$ oxygen-deficient perovskite (LP-$Ca_2AlSiO_{5.5}$) was synthesized and determined as an intermediate structure between $Ca_2Si_2O_6$ cubic perovskite and $Ca_2Al_2O_5$ brownmillerite-type phase [13,15]. The crystal structure of LP-$Ca_2AlSiO_{5.5}$ was further refined based on NMR measurements and synchrotron powder X-ray diffraction patterns [16]. Their refinement showed that LP-$Ca_2AlSiO_{5.5}$ consists of a perovskite-like layer of (Al,Si)O_6 octahedra and double layers of SiO_4 tetrahedra, stacked alternatively in the [111] direction of cubic perovskite. On the other hand, the phase boundary between LP-$Ca_2AlSiO_{5.5}$ and HP-$Ca_2AlSiO_{5.5}$ was constrained up to 23 GPa and 1873 K [17]. The physical properties of LP-$Ca_2AlSiO_{5.5}$ and HP-$Ca_2AlSiO_{5.5}$ were investigated by in-situ X-ray diffraction measurements under high pressures [18].

However, the effect of temperature on the crystal structures and physical properties of LP-$Ca_2AlSiO_{5.5}$ and HP-$Ca_2AlSiO_{5.5}$ has not been

* Corresponding author.
E-mail address: zhaishuangmeng@mail.gyig.ac.cn (S. Zhai).

https://doi.org/10.1016/j.vibspec.2019.102935
Received 26 December 2018; Received in revised form 6 May 2019; Accepted 12 June 2019
Available online 13 June 2019
0924-2031/

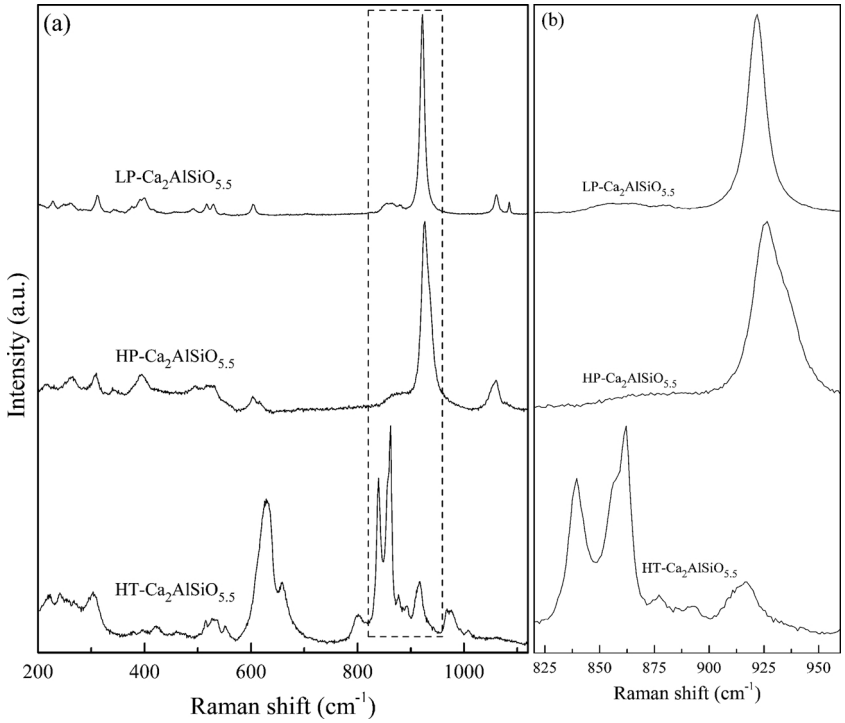

Fig. 1. Raman spectra of $Ca_2AlSiO_{5.5}$ polymorphs at ambient conditions. The right figure shows the enlarged Raman spectra between 820 and 960 cm^{-1}.

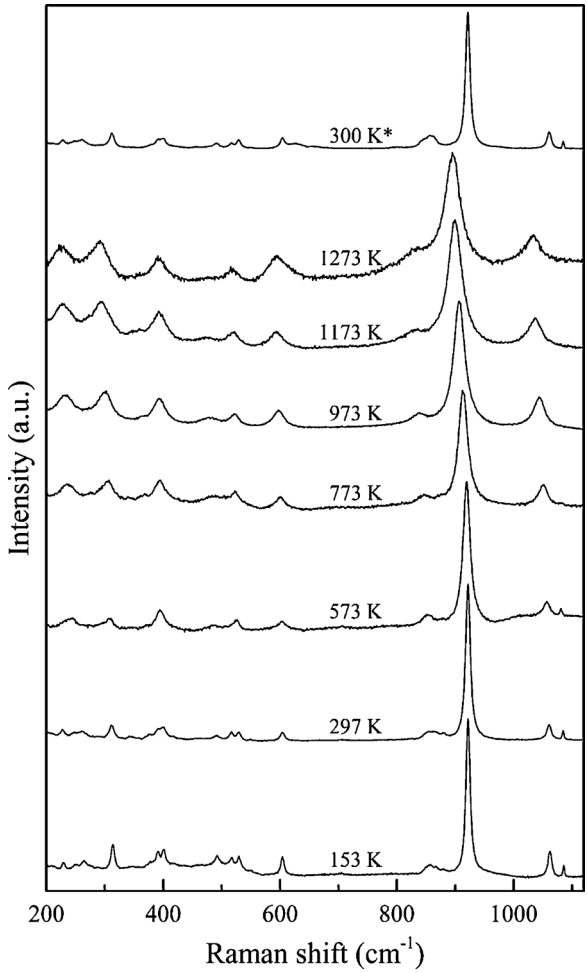

Fig. 2. Typical Raman spectra of low-pressure $Ca_2AlSiO_{5.5}$ at various temperatures and ambient pressure.

studied. It is known that Micro-Raman spectroscopy is a powerful tool to obtain the vibrational information of atoms for studying a crystal structure [19]. In this paper we firstly report the Micro-Raman spectra of LP-$Ca_2AlSiO_{5.5}$ and HP-$Ca_2AlSiO_{5.5}$ at temperatures ranging from 153 to 1273 K at ambient pressure. A temperature-induced irreversible phase transition for HP-$Ca_2AlSiO_{5.5}$ was observed at 1223 K to form a single phase whose Raman spectra were also investigated in the temperature range of 153–1273 K at ambient pressure. The temperature-dependent Raman active modes of $Ca_2AlSiO_{5.5}$ polymorphs were quantitatively analyzed and the isobaric mode Grüneisen parameters of LP-$Ca_2AlSiO_{5.5}$ were calculated.

2. Experimental details

According to the study of Kojitani et al. [17], LP-$Ca_2AlSiO_{5.5}$ was synthesized at 10 GPa and 1573 K, and HP-$Ca_2AlSiO_{5.5}$ was synthesized at 15 GPa and 1673 K. The Raman spectra at ambient pressure and various temperatures were collected in the frequency range of 200 ~ 1200 cm^{-1} *via* a Raman spectroscope (Horiba LabRam HR Evolution) equipped with an 1800 gr/mm grating. The spectrometer was calibrated by plasma and neon emission lines and the precision of the frequency determination was about 1 cm^{-1}. A YAG: Nd^{3+} laser was used as exciting source with a wavelength of 532 nm and a power of 20 mW for the sample. An SLM Plan 20× Olympus microscope objective was used to focus the laser beam and collect the scattered light. The powdered sample was pressed into a small thin bit and put on a sapphire or silica window for the high-temperature or low-temperature Raman spectroscopic measurements, respectively. The sapphire window was put into an alumina chamber in a Linkam TS 1500 for heating, while the silica window was placed at the center of a small silver block for freezing runs using THMSG 600. In high-temperature measurements, a resistance heater was used along with a water cooling system and an S-type thermocouple was used. In low-temperature measurements, liquid nitrogen was pumped through an annulus in the silver block and a resistance heater opposes the cooling effect of the nitrogen to yield the desired temperature. In both modes, the temperature control unit is completely automatic and can be programmed

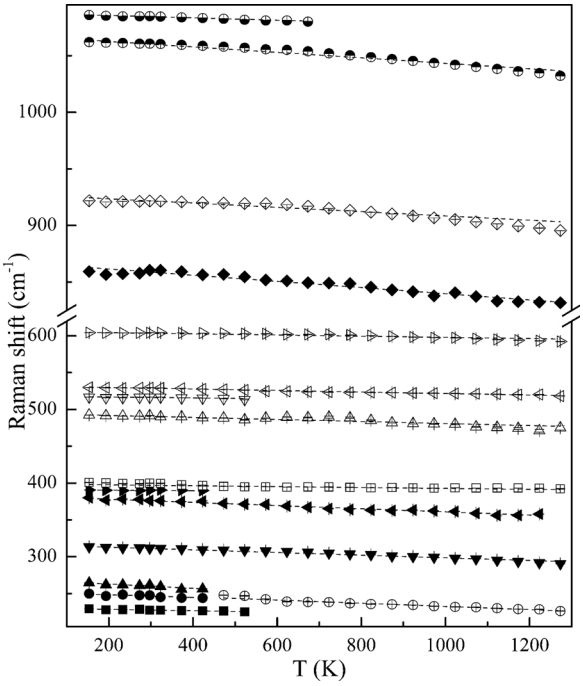

Fig. 3. Temperature dependence of the Raman bands of low-pressure $Ca_2AlSiO_{5.5}$ at ambient pressure.

to maintain at desired temperatures or change temperature at a constant rate of 10 K/min. The measurement system has been calibrated at both high and low temperatures by observing phase changes in synthetic fluid inclusions placed in the center of the crucible. Horizontal thermal gradients may have errors of up to 1% in temperature measurements. For thermal equilibrium, the spectra were collected after dwelling at the desired temperatures for 10~15 min. The accumulation time for each spectrum was 60 s, and the final spectrum was the average of three collections. The Raman shift of each band was fitted by using the PeakFit program (SPSS Inc., Chicago).

3. Results and discussion

3.1. Raman spectra at ambient conditions

As mentioned above, the crystal structures of LP-$Ca_2AlSiO_{5.5}$ and HP-$Ca_2AlSiO_{5.5}$ have been characterized. LP-$Ca_2AlSiO_{5.5}$ is in monoclinic structure with a space group of *C*2 and Z = 16, in which all Si and Al reside in tetrahedral and octahedral sites, respectively [16]. The Raman active vibrations of LP-$Ca_2AlSiO_{5.5}$ were predicted by symmetry-adapted modes [20], yielding the following modes:

$\Gamma = 55A + 56B.$

Therefore, totally 111 Raman vibrational modes are predicted for LP-$Ca_2AlSiO_{5.5}$. For HP-$Ca_2AlSiO_{5.5}$, its crystal structure is not well constrained due to the lack of space group and detailed atoms sites though the Si and Al distribute randomly in octahedral sites [14]. So it is difficult to predict the Raman active modes of HP-$Ca_2AlSiO_{5.5}$.

The Raman spectra of LP-$Ca_2AlSiO_{5.5}$ and HP-$Ca_2AlSiO_{5.5}$ at ambient conditions are shown in Fig. 1(a). Due to the very low intensity of some modes, the number of observed Raman vibrations for LP-$Ca_2AlSiO_{5.5}$ is fewer than the predicted. Both LP-$Ca_2AlSiO_{5.5}$ and HP-$Ca_2AlSiO_{5.5}$ show a strong peak at around 925 cm^{-1}, but the position and shape are slight different, as illustrated in Fig. 1(b). It is impossible to assign the peaks to different Raman modes without theoretical simulation. However, based on previous Raman spectroscopic studies on some silicates containing SiO_4 tetrahedra, bands above 1000 cm^{-1} can be generally assigned to Si-O asymmetric stretching modes of SiO_4 and the most intense Raman band near 920-930 cm^{-1} corresponds probably to Si-O symmetric stretching mode of SiO_4 [21–27]. The Raman spectra were not analyzed by full range from 200 to 1100 cm^{-1}, but by two separated ranges of 200–700 and 750-1150 cm^{-1} for LP-$Ca_2AlSiO_{5.5}$ and three separated ranges of 200–550, 570–700 and 750-1150 cm^{-1} for HP-$Ca_2AlSiO_{5.5}$. Therefore, the peaks can be located well.

Table 1
Constants determined in $\nu_i = a_i + b_i T$ at ambient pressure for $Ca_2AlSiO_{5.5}$ polymorphs.

No.	LP-$Ca_2AlSiO_{5.5}$				HP-$Ca_2AlSiO_{5.5}$			HT-$Ca_2AlSiO_{5.5}$		
	a_i	$-b_i \times 10^2$	R^2	γ_{iP}	a_i	$-b_i \times 10^2$	R^2	a_i	$-b_i \times 10^2$	R^2
1	1087.7(3)	1.06(7)	0.951	0.10	1067.7(4)	2.80(5)	0.992	1013.4(6)	2.16(21)	0.910
2	1067.4(5)	2.41(8)	0.972	0.23	1054.3(5)	1.39(22)	0.858	980.6(8)	1.97(21)	0.897
3	927.4(9)	1.89(17)	0.841	0.21	938.2(6)	1.42(14)	0.816	971.1(6)	1.50(20)	0.848
4	867.1(10)	2.73(16)	0.928	0.32	929.1(5)	1.60(16)	0.822	921.3(4)	2.16(10)	0.947
5	605.9(2)	0.80(6)	0.882	0.14	883.7(9)	3.56(14)	0.969	894.8(4)	1.25(9)	0.886
6	532.0(2)	1.04(4)	0.961	0.20	617.0(6)	0.50(8)	0.724	876.5(6)	−0.28(26)	0.712
7	518.0(7)	0.59(12)	0.807	0.12	605.2(5)	0.60(6)	0.782	862.3(2)	0.18(8)	0.726
8	494.7(3)	1.38(9)	0.909	0.29	533.4(3)	1.00(5)	0.953	854.9(2)	−0.19(8)	0.728
9	398.8(5)	0.61(8)	0.878	0.16	524.6(13)	2.49(34)	0.754	838.9(2)	−0.16(7)	0.715
10	390.9(3)	0.31(11)	0.732	0.08	496.2(5)	0.67(13)	0.732	807.8(4)	2.27(8)	0.967
11	382.4(5)	2.14(7)	0.977	0.57	393.3(4)	0.50(6)	0.743	666.0(4)	1.78(7)	0.961
12	316.5(2)	1.80(5)	0.983	0.58	313.3(3)	2.17(6)	0.986	638.1(4)	1.44(12)	0.923
13	268.7(10)	2.90(17)	0.897	1.10	270.4(6)	2.99(10)	0.975	626.8(7)	1.37(21)	0.767
14	252.0(16)	1.81(19)	0.755	0.74	222.2(12)	2.81(30)	0.823	552.9(2)	0.19(8)	0.719
15	230.4(4)	0.94(14)	0.820	0.42				538.1(3)	1.14(7)	0.900
16								527.3(6)	0.44(20)	0.712
17								514.5(2)	0.12(6)	0.690
18								465.2(4)	0.22(15)	0.710
19								424.7(8)	1.45(25)	0.788
20								398.5(10)	0.48(23)	0.603
21								378.5(18)	3.20(45)	0.807
22								310.0(4)	1.67(10)	0.916
23								273.7(10)	1.26(25)	0.797
24								260.5(9)	2.60(18)	0.869
25								245.1(6)	1.59(29)	0.802
26								227.8(3)	2.29(9)	0.977

ν_i and a_i are in cm^{-1}, T in K, b_i in cm^{-1} K^{-1}. R^2 is the correlation coefficient.

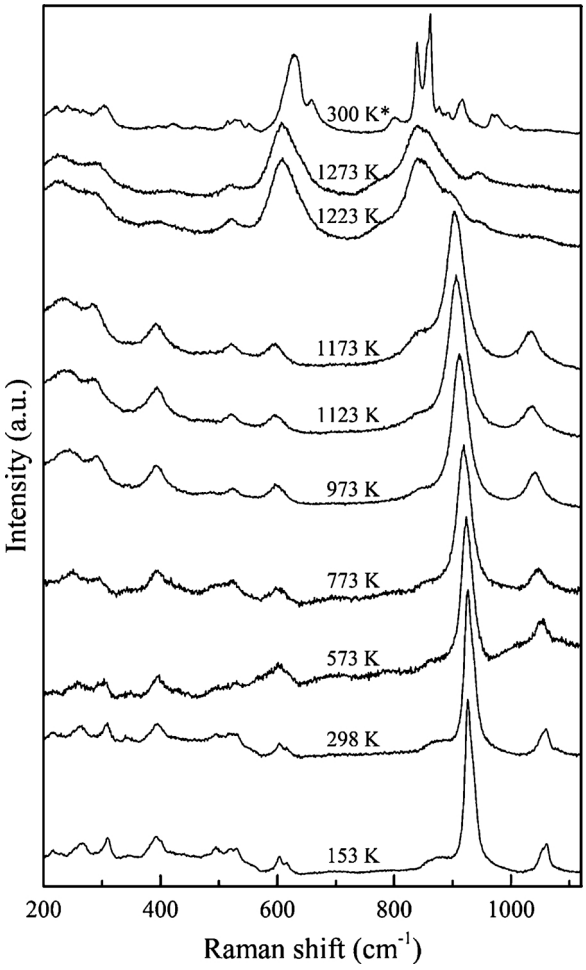

Fig. 4. Typical Raman spectra of high-pressure $Ca_2AlSiO_{5.5}$ at various temperatures and ambient pressure.

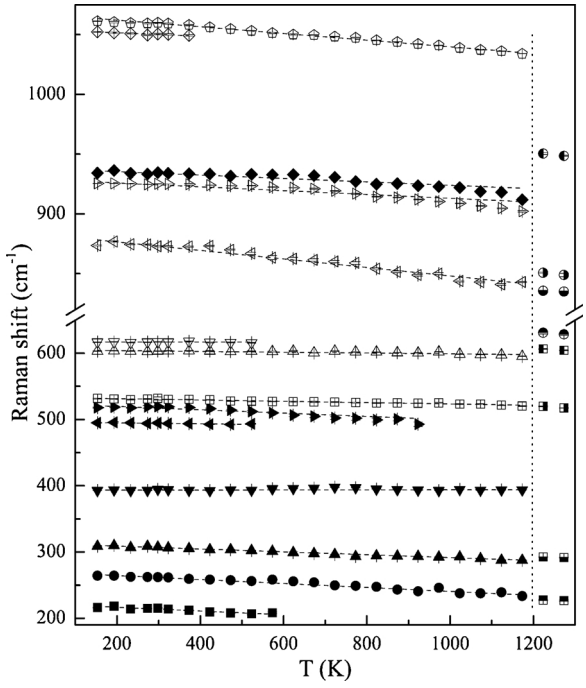

Fig. 5. Temperature dependence of the Raman bands of high-pressure $Ca_2AlSiO_{5.5}$ at ambient pressure.

3.2. Temperature-dependent Raman spectra of LP-$Ca_2AlSiO_{5.5}$

The typical Raman spectra of LP-$Ca_2AlSiO_{5.5}$ at various temperatures are plotted in Fig. 2. It is obvious that, with increasing temperature the Raman peaks of LP-$Ca_2AlSiO_{5.5}$ gradually shift to lower frequencies, which indicates an increasing bond length. This is reasonable since the bond lengths become longer with increasing temperature and longer bond lengths imply weaker bonds, *i.e.*, smaller force constant, and consequently lower vibrational frequency according to Hooke's law.

It is noted that some bands of LP-$Ca_2AlSiO_{5.5}$ become undistinguished due to the weak intensity during heating. On the other hand, two weak peaks at 248 and 261 cm^{-1} for LP-$Ca_2AlSiO_{5.5}$ at ambient conditions merge at around 473 K. Up to 1273 K, no phase transition was observed for LP-$Ca_2AlSiO_{5.5}$. The Raman spectrum at 300 K after cooling from 1273 K is same as the initial Raman spectrum of LP-$Ca_2AlSiO_{5.5}$ shown in Fig. 2 at ambient conditions.

The frequency shifts of the Raman bands of LP-$Ca_2AlSiO_{5.5}$ as a function of temperature up to 1273 K are shown in Fig. 3. Totally 15 bands could be reliably indentified. These bands all show a linear decrease in Raman shift with increasing temperature. The temperature dependences for each of the observed bands are given in Table 1, ranging from -2.90 × 10^{-2} to -0.31 × 10^{-2} cm^{-1} K^{-1}.

The temperature coefficients of the different Raman modes can be used to obtain the isobaric Grüneisen parameter, γ_{iP}, which is given as the following formula [28]:

$$\gamma_{iP} = -1/\alpha(\partial \ln \nu_i/\partial T)_P$$

where ν_i is the vibrational frequency of the *i*th band and α is the thermal expansion coefficient. The volume thermal expansion coefficient α of a material is defined as $\alpha = 1/V\ (\partial\ V/\partial\ T)_P$, and is measured experimentally by the evolution of the sample volume (in practice the unit cell volume by diffraction) with temperature. If the volume thermal expansion coefficient α does not change with temperature, then integration gives [29]:

$$\ln\ (V\ /\ V_0)\ =\ \alpha\ (T\ -\ T_0).$$

Based on the high-pressure and high-temperature X-ray diffraction data of LP-$Ca_2AlSiO_{5.5}$ reported by Xu et al. [18], the thermal expansion coefficient α can be obtained as 9.77(10) × 10^{-5} K^{-1}. The values of γ_{iP} for different modes of LP-$Ca_2AlSiO_{5.5}$ are also listed in Table 1, ranging from 0.08 to 1.10 and giving an average of 0.35. On the other hand, the bulk thermochemical Grüneisen parameter, which is equal to $\alpha KV/C_v$ (where α is the thermal expansion, K is the bulk modulus, V is the molar volume and C_v is the volume constant heat capacity), cannot be calculated for LP-$Ca_2AlSiO_{5.5}$ due to the lack of volume constant heat capacity.

3.3. Temperature-dependent Raman spectra of HP-$Ca_2AlSiO_{5.5}$

The typical Raman spectra of HP-$Ca_2AlSiO_{5.5}$ at various temperatures are illustrated in Fig. 4. Similar to those of LP-$Ca_2AlSiO_{5.5}$, the Raman bands of HP-$Ca_2AlSiO_{5.5}$ also gradually shift to lower frequency with increasing temperature. Besides, some Raman bands of HP-$Ca_2AlSiO_{5.5}$ become undistinguished due to the weak intensity during heating. Obviously, the Raman spectrum at 1223 K is quite different from that at 1173 K for HP-$Ca_2AlSiO_{5.5}$, as shown in Fig.4, which means that a temperature-induced phase transition happens. The Raman spectrum at 300 K after cooling from 1273 K is similar to that at 1273 K but totally different from the initial Raman spectrum of HP-$Ca_2AlSiO_{5.5}$ shown in Fig. 1(a) at ambient conditions, which indicates that the temperature-induced phase transition is irreversible. In particular, the strong band of HP-$Ca_2AlSiO_{5.5}$ near 930 cm^{-1} disappears and new strong bands appear around 850 and 630 cm^{-1}. Such Raman changes may indicate that at high temperature phase Al and Si atoms are no

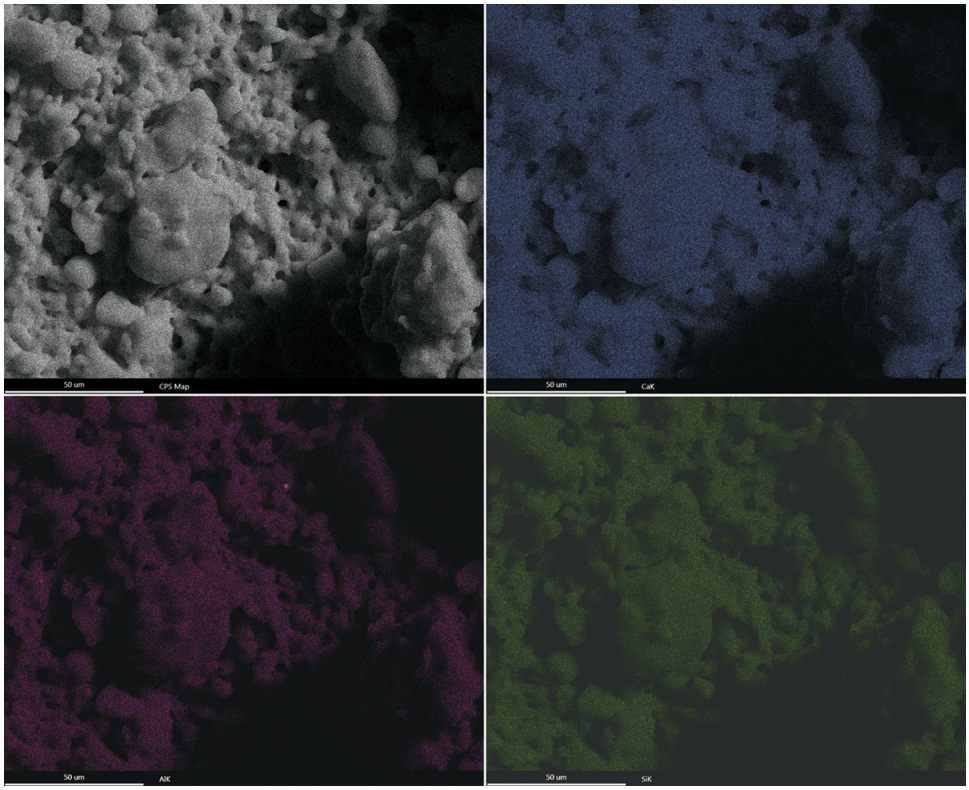

Fig. 6. Back-scattered electron image and mapping analysis of the high-temperature $Ca_2AlSiO_{5.5}$ recovered from 1273 K of high-pressure $Ca_2AlSiO_{5.5}$. The scales are the same as 50 μm.

longer randomly distributed. Further investigation is necessary to clarify the crystallographic evolution during the temperature-induced phase transformation.

The Raman shift *versus* temperature plot of HP-$Ca_2AlSiO_{5.5}$ is illustrated in Fig. 5. Totally 14 Raman active bands could be reliably indentified as a function of temperature. The Raman shifts of all modes in HP-$Ca_2AlSiO_{5.5}$ change linearly and continuously with temperature, and the slopes are different for different modes. The temperature dependences for each of the observed bands are also listed in Table 1, ranging from -3.56×10^{-2} to -0.50×10^{-2} cm^{-1} K^{-1}. Due to the lack of thermal expansive coefficient of HP-$Ca_2AlSiO_{5.5}$, the isobaric Grüneisen parameters cannot be estimated in the present study.

3.4. Temperature-dependent Raman spectra of HT-$Ca_2AlSiO_{5.5}$

The recovered sample of HP-$Ca_2AlSiO_{5.5}$ from 1273 K was then directly checked by scanning electron microscope without any polishing. As shown in Fig. 6, it is clear that the recovered sample contains a single homogeneous phase based on the mapping analysis of Ca, Al and Si elements. Therefore, it is a high-temperature $Ca_2AlSiO_{5.5}$ (HT-$Ca_2AlSiO_{5.5}$) phase. Further study on the crystal structure of this HT-$Ca_2AlSiO_{5.5}$ is required. Though the Raman active modes of HT-$Ca_2AlSiO_{5.5}$ cannot be predicted, Raman spectrum of this HT-$Ca_2AlSiO_{5.5}$ was collected at ambient conditions, as shown in Fig. 1. The Raman spectrum of HT-$Ca_2AlSiO_{5.5}$ shows three strong bands at around 623, 839 and 862 cm^{-1}, which is different from those of LP-$Ca_2AlSiO_{5.5}$ and HP-$Ca_2AlSiO_{5.5}$. Totally 26 Raman active vibrations can be distinguished for HT-$Ca_2AlSiO_{5.5}$ at ambient conditions.

The Raman spectra of HT-$Ca_2AlSiO_{5.5}$ have also been collected at various temperatures, and typical spectra were plotted in Fig. 7. With increasing temperature, some vibrations of HT-$Ca_2AlSiO_{5.5}$ become undistinguished due to the weak intensity. Besides, three mergers of peaks occur, which does not indicate any phase transition. Up to 1273 K, no phase transition was observed for HT-$Ca_2AlSiO_{5.5}$. And the Raman spectrum at 300 K after cooling from 1273 K is same as the initial Raman spectrum of HT-$Ca_2AlSiO_{5.5}$ shown in Fig. 2 at ambient conditions.

The temperature-Raman shift relations of HT-$Ca_2AlSiO_{5.5}$ are illustrated in Fig. 8. The Raman shifts of all modes in HT-$Ca_2AlSiO_{5.5}$ vary linearly and continuously with temperature, and the slopes are different for different vibrations. The temperature dependences for each of the observed modes are also listed in Table 1, ranging from -3.20×10^{-2} to 0.28×10^{-2} cm^{-1} K^{-1}. Due to the lack of thermal expansive coefficient of HT-$Ca_2AlSiO_{5.5}$, it is impossible to determine the isobaric Grüneisen parameters.

4. Conclusions

In this study, the Raman spectra of low-pressure and high-pressure $Ca_2AlSiO_{5.5}$ oxygen-deficient perovskites were collected and analyzed in the temperature region of 153–1273 K at ambient pressure. No phase transition was observed for low-pressure $Ca_2AlSiO_{5.5}$ up to 1273 K, but an irreversible temperature-induced phase transformation occurs for high-pressure $Ca_2AlSiO_{5.5}$ at 1223 K to form a high-temperature $Ca_2AlSiO_{5.5}$ phase. The Raman spectra of high-temperature $Ca_2AlSiO_{5.5}$ was also investigated in the temperature region of 153–1273 K at ambient pressure. The Raman frequencies of all observed vibrations for low-pressure, high-pressure and high-temperature $Ca_2AlSiO_{5.5}$ polymorphs continuously and linearly decrease with increasing temperature. The temperature coefficients of all Raman active modes for the three phases were quantitatively determined, ranging from -2.90×10^{-2} to -0.31×10^{-2}, -3.56×10^{-2} to -0.50×10^{-2}, and -3.20×10^{-2} to 0.28×10^{-2} cm^{-1} K^{-1} for low-pressure, high-pressure, and high-temperature $Ca_2AlSiO_{5.5}$, respectively. The calculated isobaric mode Grüneisen parameters of low-pressure $Ca_2AlSiO_{5.5}$ vary from 0.08 to 1.10 yielding an average isobaric mode Grüneisen parameter of 0.35.

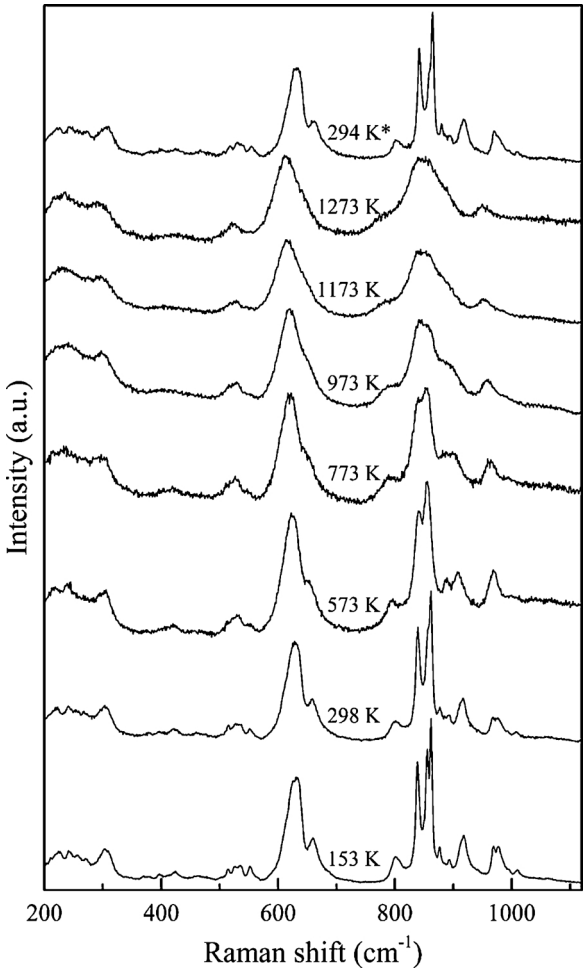

Fig. 7. Typical Raman spectra of high-temperature $Ca_2AlSiO_{5.5}$ at various temperatures and ambient pressure.

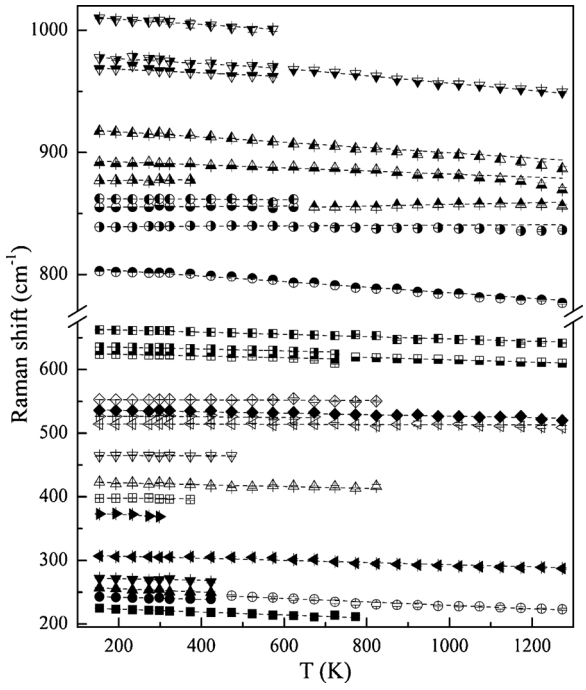

Fig. 8. Temperature dependence of the Raman bands of high-temperature $Ca_2AlSiO_{5.5}$ at ambient pressure.

Acknowledgements

The low-pressure and high-pressure $Ca_2AlSiO_{5.5}$ samples were kindly provided by H. Kojitani. The authors thank B. Mo for her help on scanning electron microscopic analysis. We thank Prof. Y. Furukawa for the editorial handling. Critical comments and suggestion from two anonymous reviewers are helpful to improve the manuscript. This work was financially supported by the National Natural Science Foundation of China (Grant No. U1532126), and the Western Light Talents Training Program of Chinese Academy of Sciences.

References

[1] H. Ye, Y. Tang, P. Li, W. Liao, J. Gao, X. Hua, H. Cai, P. Shi, Y. You, R. Xiong, Science 361 (2018) 151–155.
[2] T. Zheng, J. Wu, D. Xiao, J. Zhu, Prog. Mater. Sci. 98 (2018) 552–624.
[3] C. Rao, R. Mahesh, A.K. Raychaudhuri, R. Mahendiran, J. Phys. Chem. Solids 59 (1998) 487–501.
[4] Y. Maeno, H. Hashimoto, K. Yoshida, S. Nishizaki, T. Fujita, J.G. Bednorz, F. Lichtenberg, Nature 372 (1994) 532–534.
[5] K.I. Kobayashi, T. Kimura, H. Sawada, K. Terakura, Y. Tokura, Nature 395 (1998) 677.
[6] J.B. Philipp, D. Reisinger, M. Schonecke, A. Marx, A. Erb, L. Alff, R. Gross, J. Klein, Appl. Phys. Lett. 79 (2001) 3654–3656.
[7] M.A. Peña, J.L.G. Fierro, Chem. Rev. 101 (2001) 1981–2017.
[8] P. Roy, V. Waghmare, T. Maiti, RSC Adv. 6 (2016) 54636–54643.
[9] O. Tschauner, C. Ma, J.R. Beckett, C. Prescher, V.B. Prakapenka, G.R. Rossman, Science 346 (2014) 1100–1102.
[10] M. Lufaso, P. Woodward, Acta Crystallogr. B 57 (2001) 725–738.
[11] R.H. Mitchell, M.D. Welch, A.R. Chakhmouradian, Mineral. Mag. 81 (2017) 411–461.
[12] A. Navrotsky, Science 284 (1999) 1788–1789.
[13] U. Bläß, F. Langenhorst, D. Frost, F. Seifert, Phys. Chem. Miner. 34 (2007) 363–376.
[14] J. Fitz Gerald, A. Ringwood, Phys. Chem. Miner. 18 (1991) 40–46.
[15] U. Bläß, F. Langenhorst, T. Boffa-Ballaran, F. Seifert, D. Frost, C. McCammon, Phys. Chem. Miner. 31 (2004) 52–65.
[16] M. Kanzaki, X. Xue, Y. Wu, S. Nie, Phys. Chem. Miner. 44 (2017) 717–733.
[17] H. Kojitani, Y. Wakabayashi, Y. Tejima, C. Kato, M. Haraguchi, M. Akaogi, Phys. Earth Planet. Inter. 173 (2009) 349–353.
[18] C. Xu, S. Zhai, L. Ye, Y. Higo, Phys. Chem. Miner. 42 (2015) 327–336.
[19] P.F. McMillan, A. Hofmeister, Rev. Mineral. Geochem. 18 (1988) 99–159.
[20] E. Kroumova, M.I. Aroyo, J.M. Perez Mato, A. Kirov, C. Capillas, S. Ivantchev, H. Wondratschek, Phase Transit. A Multinatl. J. 76 (2003) 155–170.
[21] K. Iishi, Am. Mineral. 63 (1978) 1198–1208.
[22] B. Piriou, P. McMillan, Am. Mineral. 68 (1983) 426–443.
[23] F. Guyot, H. Boyer, M. Madon, B. Velde, J.P. Poirier, Phys. Chem. Miner. 13 (1986) 91–95.
[24] A. Chopelas, Am. Mineral. 76 (1991) 1101–1109.
[25] A.M. Hofmeister, A. Chopelas, Phys. Chem. Miner. 17 (1991) 503–526.
[26] E. Huang, C.H. Chen, T. Huang, E.H. Lin, J. Xu, Am. Mineral. 85 (2000) 473–479.
[27] T. Mouri, M. Enami, J. Mineral. Petrol. Sci. 103 (2008) 100–104.
[28] P. Gillet, F. Guyot, J.M. Malezieux, Phys. Earth Planet. Inter. 58 (1989) 141–154.
[29] Y. Fei, T.J. Ahrens (Ed.), Mineral Physics & Crystallography: A Handbook of Physical Constants, American Geophysical Union, Washington DC, 1995, pp. 29–44.